Arteriosclerosis, Thrombosis, and Vascular Biology

BASIC SCIENCES

Angiocrine FSTL1 (Follistatin-Like Protein 1) Insufficiency Leads to Atrial and Venous Wall Fibrosis via SMAD3 Activation

Haijuan Jiang,* Luqing Zhang,* Xuelian Liu,* Wei Sun, Katsuhiro Kato, Chuankai Chen, Xiao Li, Taotao Li, Zhiliang Sun, Wencan Han, Fujing Zhang, Qi Xiao, Zhongzhou Yang, Junhao Hu, Zhihai Qin, Ralf H. Adams, Xiang Gao, Yulong He

OBJECTIVE: Angiocrine factors, mediating the endothelial-mural cell interaction in vascular wall construction as well as maintenance, are incompletely characterized. This study aims to investigate the role of endothelial cell–derived FSTL1 (follistatin-like protein 1) in vascular homeostasis.

APPROACH AND RESULTS: Using conditional knockout mouse models, we show that loss of FSTL1 in endothelial cells (*Fstl1*^{ECKO}) led to an increase of pulmonary vascular resistance, resulting in the heart regurgitation especially with tricuspid valves. However, this abnormality was not detected in mutant mice with *Fstl1* knockout in smooth muscle cells or hematopoietic cells. We further showed that there was excessive αSMA (α-smooth muscle actin) associated with atrial endocardia, heart valves, veins, and microvessels after the endothelial FSTL1 deletion. There was also an increase in collagen deposition, as demonstrated in livers of *Fstl1*^{ECKO} mutants. The SMAD3 (mothers against decapentaplegic homolog 3) phosphorylation (pSMAD3) was significantly enhanced, and pSMAD3 staining was colocalized with αSMA in vein walls, suggesting the activation of TGFβ (transforming growth factor β) signaling in vascular mural cells of *Fstl1*^{ECKO} mice. Consistently, treatment with a TGFβ pathway inhibitor reduced the abnormal association of αSMA with the atria and blood vessels in *Fstl1*^{ECKO} mutant mice.

CONCLUSIONS: The findings imply that endothelial FSTL1 is critical for the homeostasis of vascular walls, and its insufficiency may favor cardiovascular fibrosis leading to heart failure.

VISUAL OVERVIEW: An online visual overview is available for this article.

Key Words: endothelial cell ■ fibrosis ■ heart failure ■ homeostasis ■ mice

Vascular endothelial cells (ECs) provide structural support for blood circulation by lining the inner layer of tubular vessels and also actively participate in the assembly of the vascular network during organogenesis by secreting various angiocrine factors.[1] For example, endothelial-derived PDGF-B (platelet-derived growth factor subunit B) was required for recruiting mural cells expressing PDGFRβ (platelet-derived growth factor receptor beta).[2,3] Mural cells are essential components of blood vascular walls, including pericytes in microvessels and smooth muscle cells (SMCs) in large blood vessels. They exert important roles in vascular function and homeostasis.[4] TGFβ (transforming growth factor β) signaling, a crucial pathway for vascular development, is involved in the regulation of mural cell proliferation and differentiation from mesenchymal cells.[5] Disruption of key components in the TGFβ pathway, including TGFBR2 (transforming growth factor beta receptor II) and ALK5 (activin receptor-like kinase 5),[6] ALK1,[7,8] endoglin,[9] and the downstream SMAD4 (mothers against decapentaplegic homolog 4) and SMAD5,[10,11] leads to vascular abnormalities including the defective mural cell recruitment. However, TGFβ 1 was also shown to be a key

Correspondence to: Yulong He, PhD, Cyrus Tang Hematology Center, Soochow University199 Ren-Ai Rd, Suzhou 215123, China. Email heyulong@suda.edu.cn
*These authors contributed equally to this article.
The Data Supplement is available with this article at https://www.ahajournals.org/doi/suppl/10.1161/ATVBAHA.119.313901.
For Sources of Funding and Disclosures, see page 971.

Arterioscler Thromb Vasc Biol is available at www.ahajournals.org/journal/atvb

Nonstandard Abbreviations and Acronyms

ALK	activin receptor-like kinase
EC	endothelial cell
ECKO	endothelial cell–specific knockout
FSTL1	follistatin-like protein 1
HCKO	hematopoietic cell–specific knockout
P	postnatal day
PECAM1	platelet endothelial cell adhesion molecule-1
SMC	smooth muscle cell
SMCKO	smooth muscle cell–specific knockout
TGFβ	transforming growth factor β
αSMA	α-smooth muscle actin

mediator in tissue fibrosis, a pathophysiological response of tissues to an insult by the recruitment of inflammatory cells, the activation of myofibroblasts and the deposition of extracellular matrix in the affected tissues.[12–15]

FSTL1 (follistatin-like protein 1), also known as TSC36 [TGF-β–induced clone 36] or FRP [follistatin-related protein]) is a secreted glycoprotein, which was first identified as a TGF-β1 inducible factor.[16] FSTL1 is expressed by many types of cells, including ECs and SMCs,[17–19] and exerts biological functions in various tissues in development and diseases.[20] In the circulatory system, it has been reported that FSTL1 is cardioprotective and epicardial FSTL1 was shown to stimulate the division of preexisting cardiomyocytes in animal models with myocardial infarction.[19,21–23] FSTL1 has also been shown to promote angiogenesis and flow recovery in an ischemic hindlimb mouse model[24] and suppressed apoptosis in cultured ECs via AKT (protein kinase B [PKB])-mediated signaling.[24,25] At the molecular level, FSTL1 was also reported to modulate the BMP (bone morphogenetic protein) and TGFβ mediated signaling pathway.[26–30]

Although both vascular ECs and SMCs express high levels of FSTL1, little is known about the differential requirement of specific cell-derived FSTL1 in blood vascular formation and maintenance. We found in this study that deletion of *Fstl1* in ECs, but not in SMCs or blood cells, led to an increase of atria- as well as vein-associated αSMA (α-smooth muscle actin)-positive cells in several organs examined. Vascular smooth muscle tissues participate in the regulation of peripheral blood pressure via their contraction and relaxation. The pathological vascular remodeling would increase the vascular resistance as reflected by the occurrence of heart regurgitation, leading ultimately to the heart failure of *Fstl1*^{ECKO} mice.

Highlights

- Loss of endothelial but not smooth muscle cell–derived or hematopoietic cell–derived FSTL1 (follistatin-like protein 1) led to an increase of pulmonary vascular resistance and tricuspid regurgitation.
- Occurrence of fibrosis with atrial endocardia, heart valves, veins, and microvessels after the endothelial FSTL1 deletion.
- Increase of SMAD3 phosphorylation (pSMAD3) and its colocalization with αSMA in vein walls, suggesting the activation of TGFβ (transforming growth factor β) signaling in vascular mural cells of *Fstl1*^{ECKO} mice.
- Partial suppression of the TGFβ pathway ameliorated the blood vessel and atria-associated fibrosis in the *Fstl1*^{ECKO} mice.

MATERIALS AND METHODS

The authors declare that all supporting data are available within the article (and its Data Supplement).

Animal Work

All animal experiments were performed in accordance with the institutional guidelines of Soochow University Animal Center. All the mice used in this study were housed in a specific pathogen-free animal facility with a 12/12 hours dark/light cycle and were free to food and water access. Normal mouse diet (Suzhou Shuangshi Experimental Animal Feed Technology, Co, Ltd) and cage bedding (Suzhou Baitai Laboratory Equipment, Co, Ltd) were used. Conditional knockout mice targeting *Fstl1* gene (*Fstl1*^{Flox}) were generated as previously described.[31] *Fstl*$^{+/-}$ mice were obtained by crossing of *Fstl1*^{Flox} mice with EIIA-Cre mice.[32] *Tek-Cre* mice (also known as TIE2-Cre[33]) were used in this study to generate the EC-specific *Fstl1* knockout (ECKO) mouse models (*Fstl1*$^{Flox/-}$*;Tek-Cre*, named *Fstl1*^{ECKO}). In addition to mediate gene deletion in ECs, the *Tek-Cre* line has recombinase activity in hematopoietic cells,[33] as also elegantly reviewed by Payne et al.[34] For the lineage-tracing studies, we introduced *ROSA*$^{mT/mG}$ (The Jackson Laboratory, Stock No. 007576) allele into the *Fstl1* mutant mice. αSMA-Cre and Vav-iCre (an optimized variant of Cre recombinase) mouse lines were used for *Fstl1* deletion in SMCs (SMC-specific knockout [SMCKO]; *Fstl1*$^{Flox/-}$*;αSMA-Cre*,[35] named *Fstl1*^{SMCKO}) or hematopoietic cells (HCKO; *Fstl1*$^{Flox/-}$*;Vav-iCre*,[36] named *Fstl1*^{HCKO}). The *αSMA-Cre* could also mediate gene deletion in non-SMC cells, including myofibroblasts, and the limitations of the SMC-Cre lines are elegantly reviewed by Chakraborty et al.[37] For the survival curve and vascular phenotype analysis, both male and female mice were used. To examine the floxed allele, Forward primer CTCCCACCTTCGCCTCTAAC and Reverse primer ATTTCTGCTCCTAGCGTGCC were used to amplify a 400 bp fragment for the wild-type (WT) allele and a 506 bp fragment for the floxed allele. For the genotyping of *Fstl1*$^{+/-}$ mice, primers used are as follows: Forward primer CTCCCACCTTCGCCTCTAAC, Reverse primer CGGCTAGGAAAGACTTGGAA. The WT allele gives a product of 635 bp, and the knockout allele gives a band of 341 bp. Cre mice were genotyped using the following primers (Forward CAACGAGTGATGAGGTTCGCAAG and Reverse TGATCCTGGCAATTTCGGCTATAC).

Echocardiography

Echocardiography of FSTL1 mutant and control mice at postnatal day (P) 10 to 17 (P10–P17) was performed using a Vevo 2100 ultrasound system (VisualSonics). Mice were anesthetized with isoflurane at 3% for induction and at 1% to 1.5% for maintenance. Skin hairs of chest regions were removed. For the analysis of heart function, peak tricuspid regurgitation velocity was measured using pulsed-wave Doppler, and the highest velocity recorded from multiple views was used, including apical 4-chamber, parasternal, and subcostal views.

Immunostaining

For whole-mount immunostaining, tissues were harvested, fixed in 4% paraformaldehyde, blocked with 3% (w/v) milk in PBS-TX (0.3% Triton X-100), and incubated with primary antibodies overnight at 4°C. For the frozen tissue section staining, tissues were collected and fixed in 4% paraformaldehyde for 2 hours at 4°C,followed by the incubation in 20% sucrose overnight before being embedded in optimal cutting temperature (OCT). Frozen sections of 10 μm were used. The antibodies used were rat anti-mouse PECAM1 (platelet endothelial cell adhesion molecule-1; 553370; BD Pharmigen), Cy3-αSMA (Sigma C6198) or eFluor 660-αSMA (50976082; eBioscience), Endomucin (14-5851; eBioscience), pSMAD3 (ab52903; Abcam),[38] and FSTL1 (AF1738; R&D). Appropriate Alexa 488, Alexa594 (Invitrogen) conjugated secondary antibodies were used. All fluorescently labeled samples were mounted and analyzed with a confocal microscope (Olympus Flueview 1000) or Leica MZ16F fluorescent dissection microscope.

Quantitative Real-Time Reverse Transcription-Polymerase Chain Reaction

Lung tissues from *Fstl1* mutant and control mice were collected and homogenized in Trizol (Ambion). RNA extraction and reverse transcription (RT) were performed following standard procedures (RevertAid First Strand cDNA Synthesis Kit, Thermo Scientific). Quantitative real-time RT-PCR (polymerase chain reaction) was performed using the SYBR premix Ex Taq kit (TaKaRa). Briefly, for each reaction, 50 ng of total RNA was transcribed for 2 min at 50°C and a denaturing step at 95°C for 30 s, then followed by 40 cycles of 5 s at 95°C and 34 s at 60°C. Fluorescence data were collected and analyzed using ABI PRISM 7500. The primers used were as follows: FSTL1: 5′-TCTGTGCCAATGTGTTTTGTGG-3′, 5′-TGAGGTAGGTCTTGCCATTACTG-3′; GAPDH: 5′-GGTGAAGGTCGGTGTGAACG-3′, 5′-CTCGCTCCTGGAAGATGGTG-3′.

Sirius Red Staining and Hydroxyproline Quantification

Collagen deposition in tissues was analyzed by Sirius Red staining and the quantification of hydroxyproline. Briefly, tissues were collected and fixed in 4% paraformaldehyde overnight at 4°C. Paraffin sections (6 μm) were processed for staining first with hematoxylin, followed by the Picro-Sirius Red (Sigma-Aldrich) staining for 1 hour (0.5 g Direct Red 80 dissolved in 500 mL 1.3% Picric acid from Sangon, Shanghai). Sections were then washed, dehydrated, and mounted in the mounting medium for further microscopic analysis. For the measurement of tissue collagen content by the hydroxyproline quantification, liver tissues (60 mg) were subjected to the alkaline hydrolysis, and hydroxyproline concentration in the tissue lysate was determined following the manufacturer's instructions (Jiancheng, Nanjing, China) as follows: (Sample OD value—blank OD)/(standard OD—blank OD)×standard sample concentration (5 μg/mL)×total hydrolysate volume (10 mL)/tissue wet weight (mg).

Western Blot

For the analysis of FSTL1 expression and deletion efficiency, tissues were washed with ice-cold PBS and lysed in lysis buffer (1 mmol/L PMSF [phenylmethylsulfonyl fluoride], 2 mmol/L Na_3VO_4, 1× protease and phosphatase inhibitor cocktail tablets without EDTA from Roche Applied Science, 20 mmol/L Tris-HCl pH 8.0, 100 mmol/L NaCl, 10 % glycerol, 50 mmol/L NaF, 10 mmol/L β-glycerolphosphate, 5 mmol/L sodium pyrophosphate, 5 mmol/L EDTA, 0.5 mmol/L EGTA, 1% NP-40 [nonyl phenoxypolyethoxylethanol]). The lysates were incubated on ice for 0.5 hour with rotation and were clarified by centrifugation. Protein concentration was determined using the bicinchoninic acid assay protein assay kit (PIERCE). Equal amounts of protein were used for analysis. Antibodies used include goat anti-mouse FSTL1 (BAF1738; R&D), mouse anti-all αSMA (A2547; Sigma), pSMAD3 (ab52903; Abcam), pSMAD2 (3108S; Cell Signaling), tSMAD2/3 (total SMAD2/3; R&D, 3797), pSMAD1/5/8 (9511S; Cell Signaling), tSMAD1 (9743S; Cell Signaling), and mouse monoclonal to β-actin antibody (sc-47778; C4, Santa Cruz).

Blockade of TGFβ Signaling

The inhibitor for TGFβ type I receptor kinase (5 mg/mL, SB431542; Selleck) was dissolved in 2% dimethyl sulfoxide (DMSO) plus 30% polyethylene glycol (PEG) 300 in ddH2O according to the instructions of the manufacturer. The *Fstl1*^{ECKO} mice were divided into 2 groups, 1 group of mice treated with the inhibitor (20 μg/g body weight) and the other group as well as the littermate WT mice receiving the solvent as controls. All the mice received 6 injections by intraperitoneal starting from the P5 (P5, P7, P9, P11, P13, and P15). As the majority of *Fstl1*^{ECKO} mice will die before 3-week-old, all the treated and control mice were euthanized at P16 for tissue collection and further analysis.

Statistics

For the statistical analysis of multiple comparisons, the 1-way ANOVA was performed if data passed the D'Agostino-Pearson normality test, or the nonparametric Kruskal-Wallis test was used instead (GraphPad Prism 7.00). For the statistical analysis for 1-way ANOVA and Kruskal-Wallis test, Dunn multiple comparisons test or Tukey multiple comparisons test have been performed as post hoc tests. For the 2-group comparison, the unpaired *t* test was performed if data passed the above normality test, or the unpaired nonparametric Mann-Whitney test was applied using Prism. All statistical tests were 2-sided.

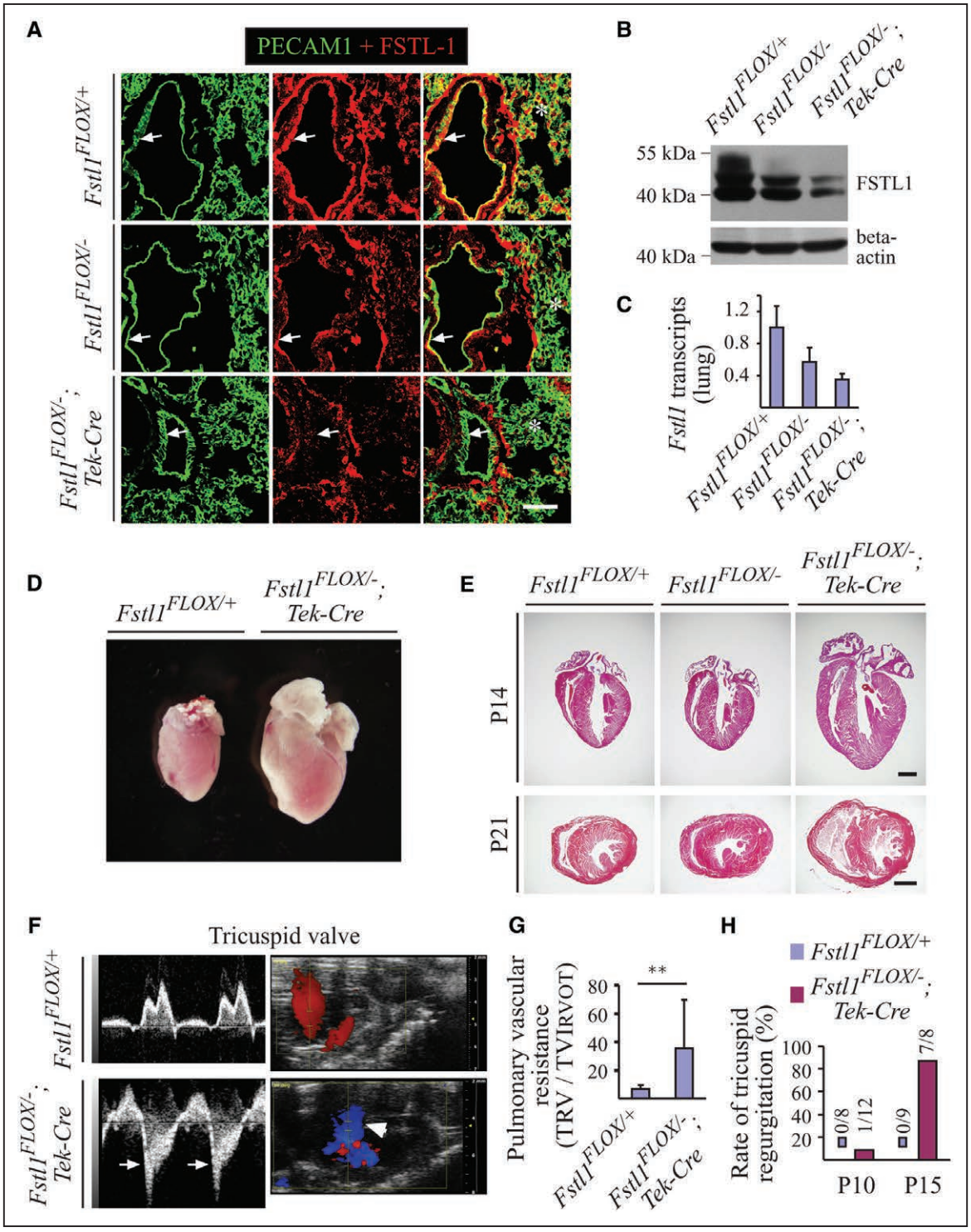

Figure 1. Analysis of FSTL1 (follistatin-like protein 1) expression in endothelial cells and heart regurgitation after the endothelial cell–specific deletion of *Fstl1*.

A, Immunostaining for PECAM1 (platelet endothelial cell adhesion molecule-1) and FSTL1 to examine the expression of FSTL1 in blood vascular endothelial cells and its deletion efficiency in the lung (green for PECAM1, and red for FSTL1). Arrows point to endothelium of large vessels and asterisks to the immunostaining signals for FSTL1 in microvessels. **B**, Western blot analysis of FSTL1 in the lung of *Fstl1*^{ECKO} mutant and control mice. **C**, Quantitative reverse transcription-polymerase chain reaction (PCR) analysis of *Fstl1* transcripts in lung from *Fstl1*$^{Flox/-}$*;Tek-cre* (*Fstl1*^{ECKO}) and littermate control mice. **D** and **E**, Cardiac hypertrophy in *Fstl1*^{ECKO} mice at the postnatal day (P) 21 (P21, **D**) and histological analysis of hearts from *Fstl1*^{ECKO} and control mice at the P14 and P21 (**E**). **F** and **G**, Analysis of heart function by In vivo ultrasonic imaging (**F**, P15–P17) and quantification of pulmonary vascular resistance in *Fstl1*^{ECKO} mice (**G**, P15). Blue signals in **F** indicate the backflow of blood in the right ventricle (arrows). **H**, Rate of tricuspid regurgitation at P10 and P15. Note that the tricuspid regurgitation was rare at P10 but occurred in most *Fstl1* mutant mice at P15 (**G**). Scale bar: 50 μm in **A**; 1000 μm in **E**. TRV indicates tricuspid regurgitation velocity; and TVI_{RVOT}, right ventricular outflow time-velocity integral.

RESULTS

Tricuspid Regurgitation Of Mutant Mice With Endothelial *Fstl1* Deletion

As mice null for *Fstl1* died at birth,[27,28] we generated the mice with *Fstl1* deletion in ECs using the *Tek-Cre* transgenic line (*Fstl1*$^{Flox/-}$*;Tek-Cre*, named *Fstl1*^{ECKO}).[33] Consistent with the previous findings,[39] we showed that FSTL1 was highly expressed by ECs (Figure 1A through 1C). *Fstl1* deletion in ECs was examined by immunostaining for PECAM1 and FSTL1 (Figure 1A, arrows), Western blot analysis (Figure 1B), and quantitative RT-PCR (Figure 1C). The relative level of *Fstl1* transcripts in mutant lung was reduced to about 35% of the WT control (*Fstl1*$^{Flox/+}$: 1.0±0.27, n=7; *Fstl1*$^{Flox/-}$, 0.57±0.18, n=6; *Fstl1*^{ECKO}: 0.35±0.07, n=8). In contrast to the complete *Fstl1* knockout mice, *Fstl1*^{ECKO} mice showed lethality starting approximately from the P10. Detailed analysis of the survival rate revealed that about 70% of *Fstl1*^{ECKO} mice died by the age of 3-week-old, and there was no significant difference between male and female mutants (Figure IA in the Data Supplement).

Further analysis revealed that the hearts of *Fstl1*^{ECKO} mice became enlarged (Figure 1D), as also demonstrated by the histological analysis at both P14 and P21 (Figure 1E) and the functional analysis at P10 and P15 to P17 by the ultrasound imaging system (VisualSonics Vevo 2100, Figure 1F through 1H). There was a significant increase of heart to body weight ratio in *Fstl1*^{ECKO} mice compared with littermate controls (*Fstl1*$^{Flox/+}$: 0.79±0.13%, n=10; *Fstl1*$^{Flox/-}$: 0.78±0.06%, n=8; *Fstl1*^{ECKO}: 1.48±0.55%, n=7; *Fstl1*^{ECKO} versus *Fstl1*$^{Flox/+}$: *P*=0.0004). The pulmonary vascular resistance was calculated by tricuspid regurgitant velocity/right ventricular outflow time-velocity integral. WT mice normally have a pulmonary vascular resistance value <10.[40] We found that there was a significant increase of pulmonary vascular resistance in *Fstl1*^{ECKO} mice at P15 (Figure 1G; *Fstl1*$^{Flox/+}$: 6.58±2.85, n=9; *Fstl1*^{ECKO}: 35.56±34.15, n=7; *P*=0.0021). The alteration of vascular resistance was also demonstrated by the observation that most of the mutant mice (7 out of 8 mice) showed tricuspid regurgitation at P15 (Figure 1F), whereas there was only 1 out of 12 *Fstl1*^{ECKO} mice detected at P10 (Figure 1H). Four *Fstl1*^{ECKO} mice (P15) with dilated cardiomyopathy were also analyzed for mitral valves; only one showed the mitral regurgitation, whereas all of them displayed the tricuspid regurgitation. Consistently, there was a significant increase of the right ventricle internal diameter (diastole, Figure IB in the Data Supplement; *Fstl1*$^{Flox/+}$: 0.91±0.35, n=9; *Fstl1*^{ECKO}: 1.35±0.39, n=9; *P*=0.0244) and also the right ventricular cavity area (diastole, Figure IC in the Data Supplement; *Fstl1*$^{Flox/+}$: 3.43±0.73, n=9; *Fstl1*^{ECKO}: 5.92±2.14, n=9; *P*=0.0044). There may be a trend of increase, but no significant difference was detected with the left ventricle internal diameter (*Fstl1*$^{Flox/+}$: 2.92±0.17, n=9; *Fstl1*^{ECKO}: 3.20±0.48, n=9; *P*=0.1159) and the left ventricular cavity area (*Fstl1*$^{Flox/+}$: 6.15±0.47, n=9; *Fstl1*^{ECKO}: 7.69±2.52, n=9; *P*=0.0894).

Increase of αSMA Associated With Atrial Endocardia and Valves of *Fstl1*^{ECKO} Mice

To investigate causes of the lethality with the *Fstl1*^{ECKO} mice, we examined the heart of mutant mice by immunostaining for αSMA and PECAM1. There was a dramatic increase of endocardium-associated αSMA^{+} cells in right and left atria of the *Fstl1*^{ECKO} mice (Figure 2A and 2B). Microvessels in the heart walls of the *Fstl1* mutant mice also showed an increase of αSMA staining, which is rarely detected in those of control mice (Figure 2A and 2B). Consistently, a similar change of the αSMA staining, associated with the ECs of valve leaflets, was also detected in the tricuspid and mitral valves of the *Fstl1*^{ECKO} mice (Figure 2C and 2D). However, there was no αSMA staining associated with endocardium of right and left ventricles, and there was also no obvious change of αSMA^{+} microvessels detected in the ventricular walls of the *Fstl1*^{ECKO} mice (Figure II in the Data Supplement).

To further investigate the effect of non-EC-derived FSTL1 in vascular development, we generated the doubly transgenic mice with *Fstl1* deletion in vascular mural cells, including SMCs (*Fstl1*$^{Flox/-}$*;αSMA-Cre*, named *Fstl1*^{SMCKO}) or in hematopoietic cells (*Fstl1*$^{Flox/-}$*;Vav-iCre*, named *Fstl1*^{HCKO}). FSTL1 deletion in *Fstl1*^{SMCKO} mice was examined by Western blot analysis (Figure IIIA in the Data Supplement) and quantitative RT-PCR (*Fstl1*$^{Flox/+}$: 1.0±0.17, n=5; *Fstl1*$^{Flox/-}$: 0.46±0.18, n=6; *Fstl1*^{SMCKO}: 0.30±0.07, n=7). Deletion of *Fstl1* gene in hematopoietic cells of *Fstl1*^{HCKO} mice was confirmed by the PCR genotyping of blood cells from mutant or control mice (Figure IIIB in the Data Supplement). All the *Fstl1*^{SMCKO} and *Fstl1*^{HCKO} mutant mice survived well by the age of 3-week-old. Surprisingly, SMCs are one of the major sources of FSTL1 and the SMA-Cre–mediated deletion efficiency of FSTL1 is similar to that of *Fstl1*^{ECKO} mice analyzed at the same stage. However, there were no obvious defects observed in mutant hearts (Figure IIIC in the Data Supplement) or in the SMC coverage with blood vessels of *Fstl1*^{SMCKO} mice (Figure IIIE in the Data Supplement). Also, there were no detectable heart and vascular abnormalities in *Fstl1*$^{Flox/-}$*;Vav-iCre* mice (Figure IIID and IIIF in the Data Supplement).

Excessive αSMA Association With Lung Veins and Microvessels in FSTL1 Mutant Mice

Consistent with the observation in the atria, there was an obvious increase of αSMA staining with blood vessels of lung in *Fstl1*^{ECKO} mice (Figure 3A). The alteration of αSMA expression was further validated by Western

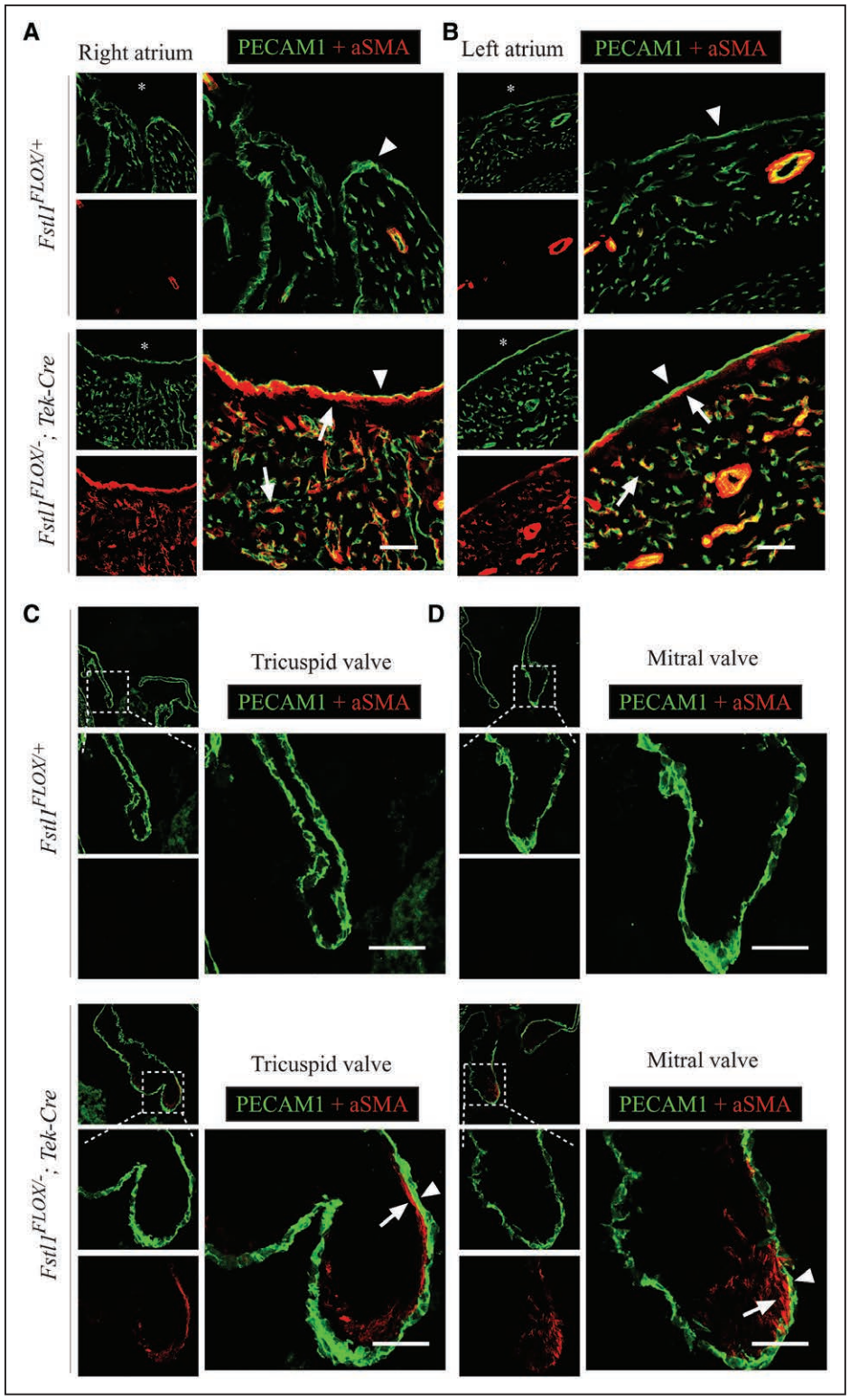

Figure 2. Increased αSMA (α-smooth muscle actin) association with the atrial endocardium and heart valves of *Fstl1*^{ECKO} mutants.

A and **B**, Immunostaining analysis of blood vessels for PECAM1 (platelet endothelial cell adhesion molecule-1; green) and αSMA (red) with right atrium (**A**), left atrium (**B**) of *Fstl1*^{ECKO} mice (postnatal day 18 [P18]). Asterisks indicate heart cavity, and arrows point to abnormal association of αSMA with endocardium (arrowheads). **C** and **D**, Analysis of tricuspid and mitral valves from *Fstl1*^{ECKO} and littermate control mice by immunostaining (P18). Arrows point to the αSMA association with valve endothelia (arrowheads). Scale bar: **A**–**D**, 50 μm.

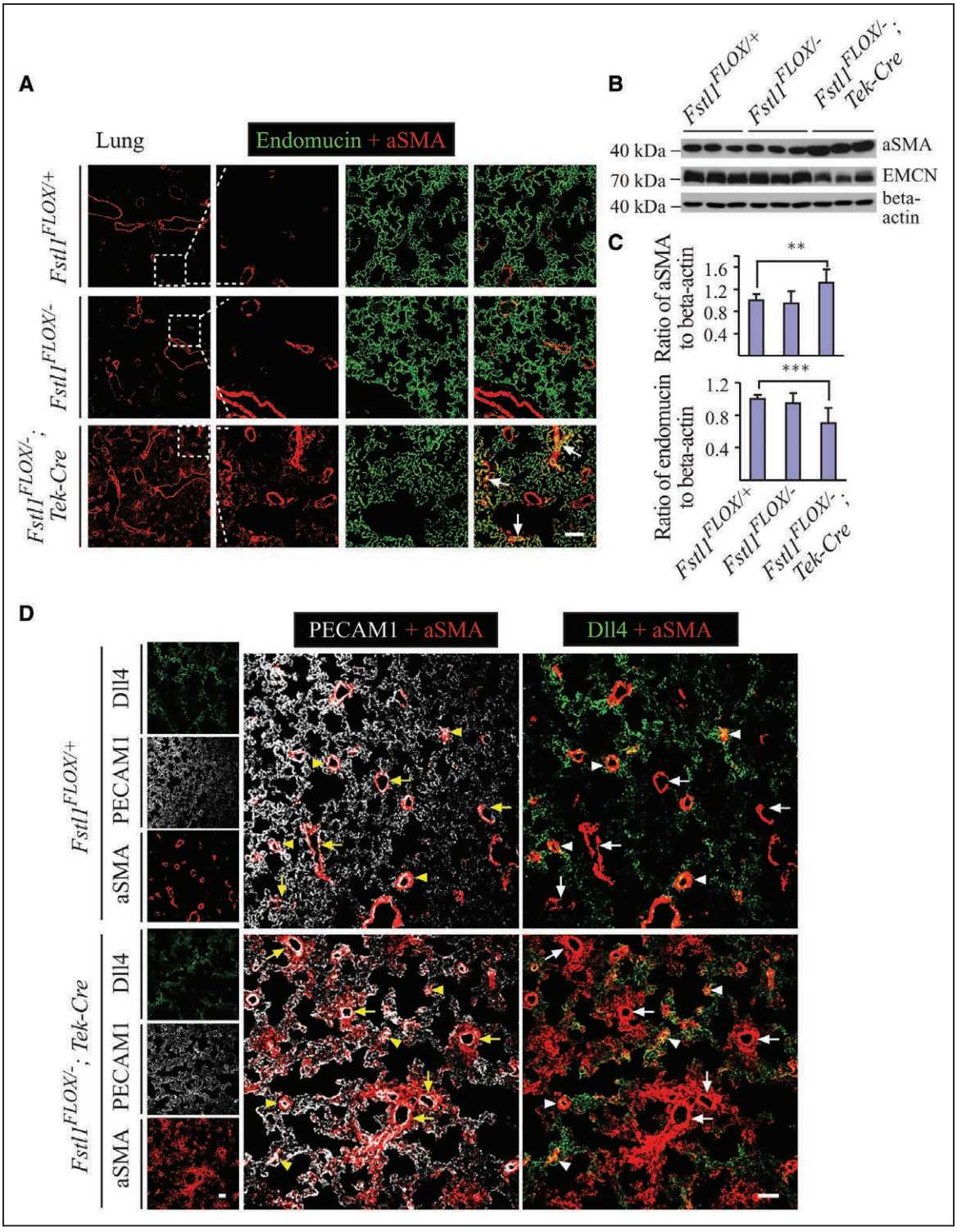

Figure 3. Upregulation of αSMA (α-smooth muscle actin) in blood vessels negative for the arterial marker Dll4 in lung of *Fstl1*^{ECKO} mice.

A, Immunostaining analysis of blood vessels for endomucin (green) and αSMA (red) with lung from *Fstl1*^{ECKO} and control mice (postnatal day 21). Arrows point to the αSMA staining in big and microvessels. **B** and **C**, Western blot analysis of αSMA and EMCN (endomucin) expression in lung from *Fstl1*^{ECKO} and littermate control mice (**B**) and quantification of the ratio of αSMA or endomucin to beta-actin, respectively (**C**). **D**, Immunostaining analysis of blood vessels for Dll4 (delta-like 4; green), αSMA (red), and PECAM1 (platelet endothelial cell adhesion molecule-1; white) with lung from *Fstl1*^{ECKO} and control mice. Arrows point to veins (Dll4 negative) and arteries (arrowheads, Dll4^{+}). Note that there is a massive increase of αSMA association with veins and microvessels, but this is not obvious with arteries at the same stage. Scale bar: 50 μm in **A** and **D**.

blot analysis in the lung of *Fstl1*^{ECKO} mice (Figure 3B). The ratio of αSMA to β-actin was quantified and normalized against the control group (Figure 3C). There was a significant increase of αSMA in *Fstl1*^{ECKO} mice compared with that of the littermate controls (Figure 3C; *Fstl1*$^{Flox/+}$: 1.0±0.11, n=7; *Fstl1*$^{Flox/-}$: 0.95±0.22, n=6; *Fstl1*^{ECKO}: 1.32±0.24, n=9; *Fstl1*^{ECKO} versus *Fstl1*$^{Flox/+}$: *P*=0.0079). Interestingly, endomucin, a membrane-bound glycoprotein expressed luminally by venous and capillary ECs, but not by arterial endothelium, was significantly decreased in lungs of the mutant mice (Figure 3C; *Fstl1*$^{Flox/+}$: 1.0±0.05, n=7; *Fstl1*$^{Flox/-}$: 0.95±0.12, n=6; *Fstl1*^{ECKO}: 0.70±0.19, n=9; *Fstl1*^{ECKO} versus *Fstl1*$^{Flox/+}$: *P*=0.0003). The decrease of endomucin level could also reflect the alteration of blood pressure.[41] Interestingly, we found that the increased αSMA was mainly associated with veins and vein-associated microvessels, which were positive for the venous and capillary EC marker endomucin (Figure 3A, arrows; lung). This was further validated by the immunostaining for Dll4, an arterial EC marker. The blood vessels with abnormal αSMA coating were negative for Dll4 (Figure 3D, arrowheads; lung).

Occurrence of Blood Vessel-Associated Fibrosis in Livers of FSTL1 Mutant Mice

We further analyzed the blood vessel-associated αSMA in several other tissues, including the liver, kidney, retina, and skin. The increase of αSMA staining was detected by immunostaining in the liver (Figure 4A), and this was confirmed by Western blot analysis (Figure 4B and 4C; *Fstl1*$^{Flox/+}$: 1.0±0.48, n=6; *Fstl1*$^{Flox/-}$: 0.84±0.10, n=3; *Fstl1*^{ECKO}: 3.45±2.17, n=6; *Fstl1*^{ECKO} versus *Fstl1*$^{Flox/+}$: *P*=0.0152). Consistent with the results observed in the lung, the protein level of endomucin was significantly decreased (Figure 4D; *Fstl1*$^{Flox/+}$: 1.0±0.30, n=6; *Fstl1*$^{Flox/-}$: 0.83±0.36, n=6; *Fstl1*^{ECKO}: 0.39±0.14, n=6; *Fstl1*^{ECKO} versus *Fstl1*$^{Flox/+}$: *P*=0.0022). An obvious increase of αSMA was also detected in kidney (Figure IV in the Data Supplement). It is worth pointing out that there was no obvious difference in αSMA level detected in the liver, lung, kidney, and heart of the *Fstl1*^{ECKO} and control mice at P1 (data not shown). By the stage of P10, 4 out of 12 *Fstl1*^{ECKO} mice displayed an increase of αSMA in the liver but not in the lung and kidney (Figure V in the Data Supplement). Quantification analysis showed that there was a trend of increase in the αSMA level in the liver but not statistically significant between the *Fstl1* mutant and control mice at P10 (liver: *Fstl1*$^{Flox/+}$ 1.0±0.43, n=6; *Fstl1*^{ECKO} 3.12±3.08, n=12; *P*=0.1797; lung: *Fstl1*$^{Flox/+}$ 1.0±0.34, n=5; *Fstl1*^{ECKO} 1.04±0.37, n=12; *P*=0.8788; kidney: *Fstl1*$^{Flox/+}$ 1.0±0.47, n=6; *Fstl1*^{ECKO} 0.94±0.23, n=12; *P*>0.9999). The variation in the vascular phenotype among organs of *Fstl1*^{ECKO} mice was also confirmed by the age of 3-week-old, with the increase of αSMA$^+$ in 14 out of 14 (14/14) livers, 10 out of 14 lungs, and 5 out of 11 kidneys examined. However, there was no obvious difference in αSMA associated with blood vessels in skin (Figure VIA in the Data Supplement) and retina tissues examined by P21 (Figure VIB in the Data Supplement). FSTL1 deficiency in EC did not produce any obvious effect on lymphatic vessel development, as shown in trachea (Figure VIC in the Data Supplement). This suggests that there may be a differential requirement of endothelial FSTL1 in the regulation of organ-specific vascular systems.

Consistent with the increase of blood vessel-associated αSMA, we also detected an increase of collagen deposition by Sirius red staining in the liver (Figure 4E), lung, and atria (Figure VIIA and VIIB in the Data Supplement) of the *Fstl1*^{ECKO} mice. This was confirmed by the quantification of hydroxyproline content in the liver tissue lysates (Figure 4F). There was a significant increase of hydroxyproline in the *Fstl1* mutant mice compared with the littermate control (*Fstl1*$^{Flox/+}$: 0.22±0.03 μg / mg, n=6; *Fstl1*^{ECKO}: 0.39±0.16 μg / mg, n=9; *P*=0.0004).

SMAD3 Activation in Vein Walls of *Fstl1*^{ECKO} Mutant Mice

To check whether there is any transition of ECs into αSMA$^+$ cells in blood vessels, we introduced ROSA$^{mT/mG}$ allele into the *Fstl1*$^{Flox/-}$*;Tek-cre* line, and the *Fstl1*$^{Flox/+}$*;Tek-cre;mT/mG* mice were used as control. Interestingly, we found that the αSMA staining was detected mainly at the outer layer of vessel walls in both large and microvessels in the liver of the *Fstl1*$^{Flox/-}$*;Tek-cre;mT/mG* mutant mice (Figure 5A). This suggests that the upregulation of αSMA occurred in perivascular mural cells. Consistent with the observations in the lung, we found that the increased αSMA was associated with veins, and microvessels, which were positive for the venous EC marker EphB4 (Figure 5B, arrows; arrowheads point to arteries).

To examine the alteration of TGFβ mediated signaling, we analyzed the phosphorylation of SMAD3 (pSMAD3) by the immunostaining (Figure 6A and 6B) and Western blot analysis (Figure 6C and 6D). The number of pSMAD3$^+$ /αSMA$^+$ doubly positive cells associated with blood vessels was significantly increased in the livers of the *Fstl1*^{ECKO} mice compared with that of littermate controls (Figure 6A and 6B; *Fstl1*$^{Flox/+}$: 1.3±0.2 / grid, n=4; *Fstl1*^{ECKO}: 7.3±1.1 / grid, n=4; *P*=0.0286). This was further confirmed by the Western blot analysis and the quantification of pSMAD3: tSMAD3 (total SMAD3) in the liver (the ratio normalized against the control, as shown in Figure 6C and 6D; *Fstl1*$^{Flox/+}$: 1.0±0.14, n=6; *Fstl1*^{ECKO}: 1.83±0.46, n=7; *P*=0.0023). The ratio of pSMAD1/5/8: tSMAD1 (total SMAD1) was not significantly altered (Figure 6D; *Fstl1*$^{Flox/+}$: 1.0±0.06, n=6; *Fstl1*^{ECKO}: 1.14±0.14, n=6; *P*=0.9372). A similar increase of SMAD3 activation was also shown by the Western blot analysis in the lung (pSMAD3 /tSMAD3: *Fstl1*$^{Flox/+}$:

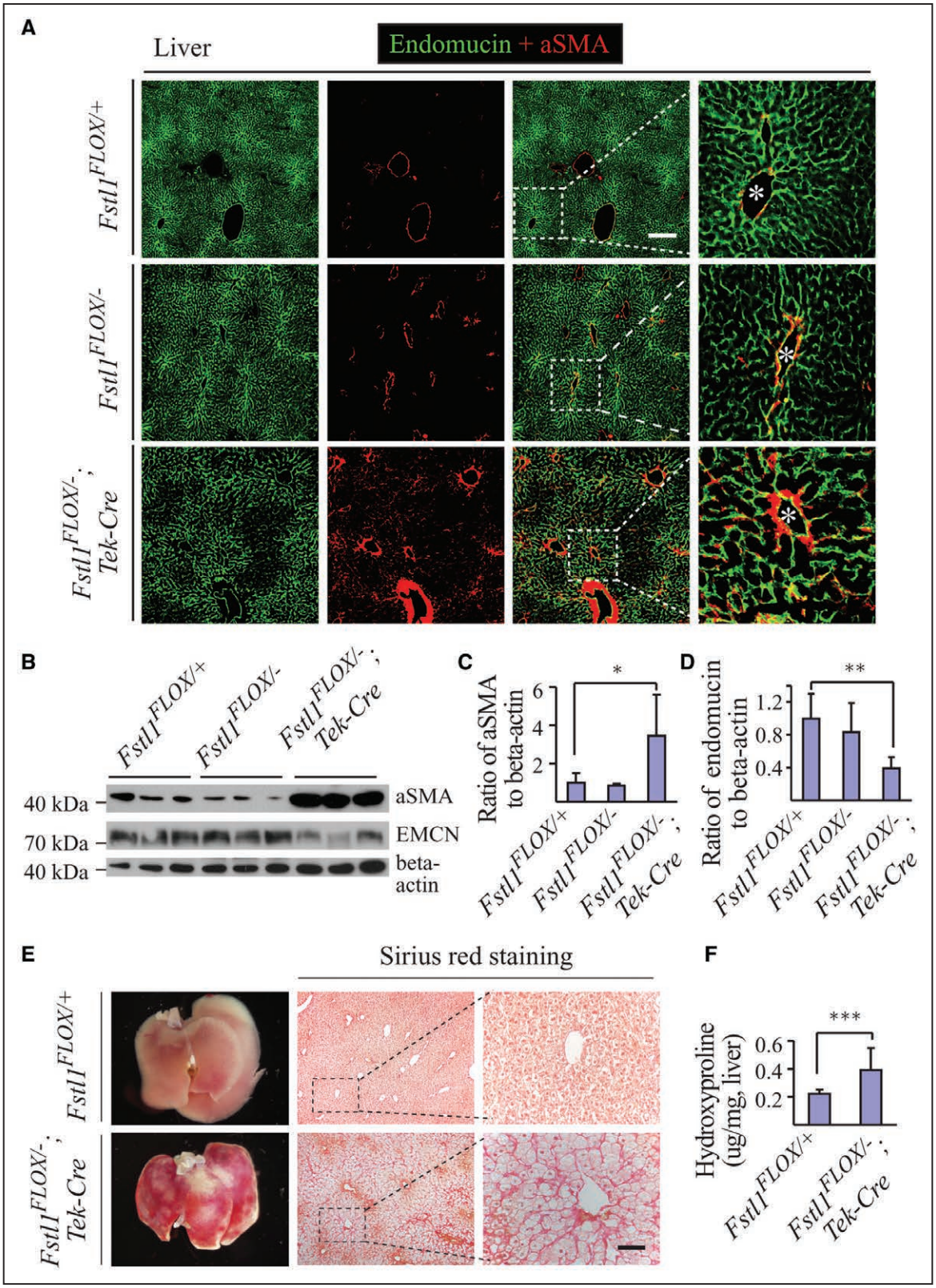

Figure 4. Occurrence of vascular fibrosis in liver of *Fstl1*^{ECKO} mutant mice.

A, Immunostaining analysis of blood vessels for endomucin (green) and αSMA (α-smooth muscle actin; red) with liver from *Fstl1*^{ECKO} mutant and littermate control mice (postnatal day 21). Asterisks point to the veins. **B**, Analysis of αSMA and EMCN (endomucin) expression in liver from *Fstl1*^{ECKO} and control mice by Western blot analysis. **C** and **D**, Quantification of the ratio of αSMA or endomucin to β-actin, respectively. **E** and **F**, Analysis of liver fibrosis by Sirius red staining (**E**) and quantification of hydroxyproline (**F**). Scale bars: 200 μm in A, 50 μm in **E**.

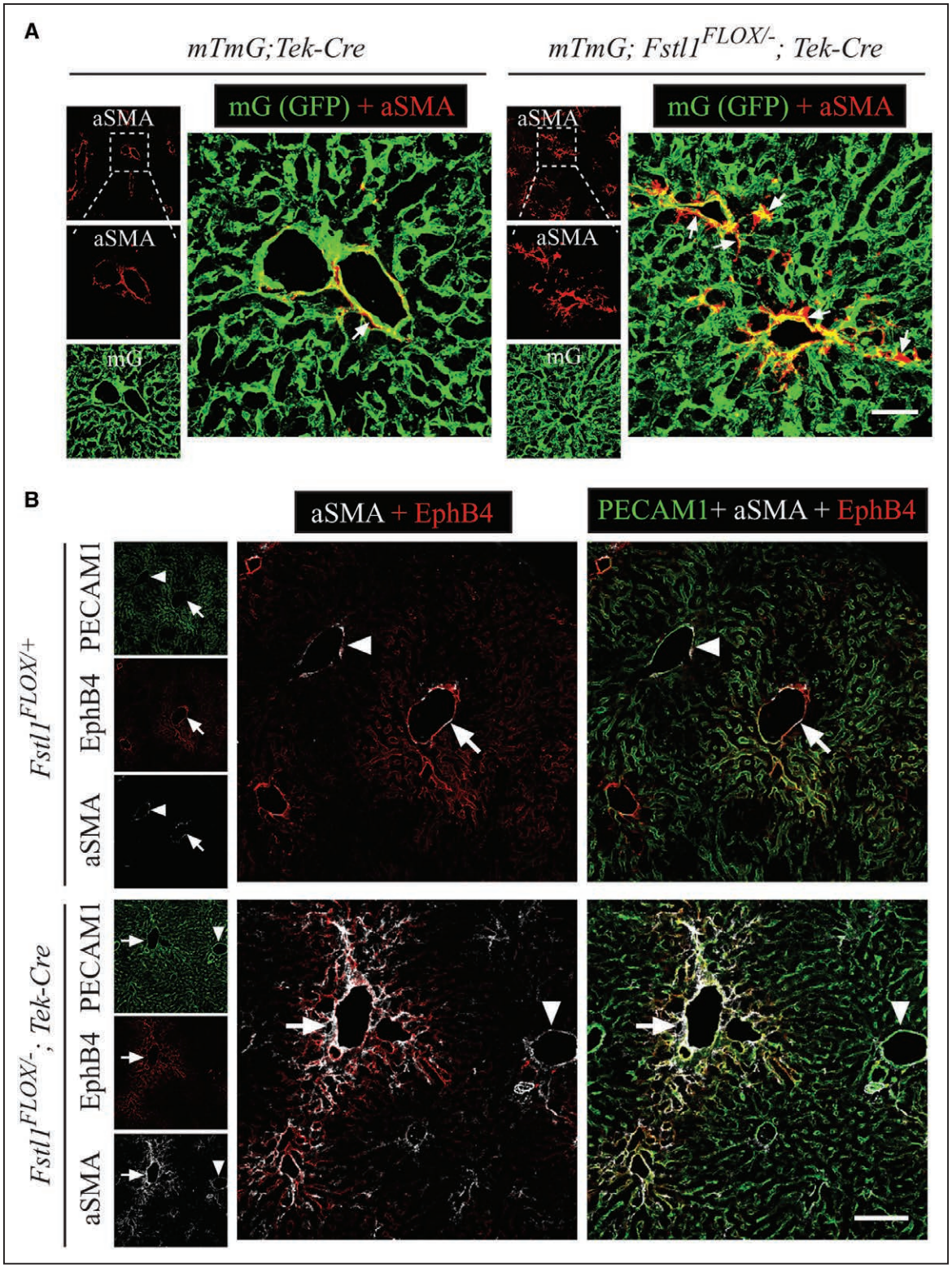

Figure 5. Association of αSMA (α-smooth muscle actin) with hepatic veins and microvessels positive for the venous marker EphB4 after the endothelial FSTL1 (follistatin-like protein 1) deletion.

A, Analysis of smooth muscle cell coverage (αSMA$^+$) with blood vessels (GFP$^+$ [green fluorescent protein]) in *mTmG* (mG, cell membrane-localized EGFP; mT, cell membrane-localized tdTomato); *Fstl1*^{ECKO} and littermate control mice at postnatal day 18. Arrows point to the large and microvessels positive for αSMA staining. **B**, Analysis of blood vessels in the liver from *Fstl1*^{ECKO} and control mice by immunostaining for PECAM1 (platelet endothelial cell adhesion molecule-1; green), EphB4 (ephrin type-B receptor 4; red), and αSMA (white). Note that αSMA mainly associated with EphB4-positive vessels (veins, arrows; arrowheads to arteries) in liver of *Fstl1*^{ECKO} mice. Scale bars: 100 μm in **A** and **B**.

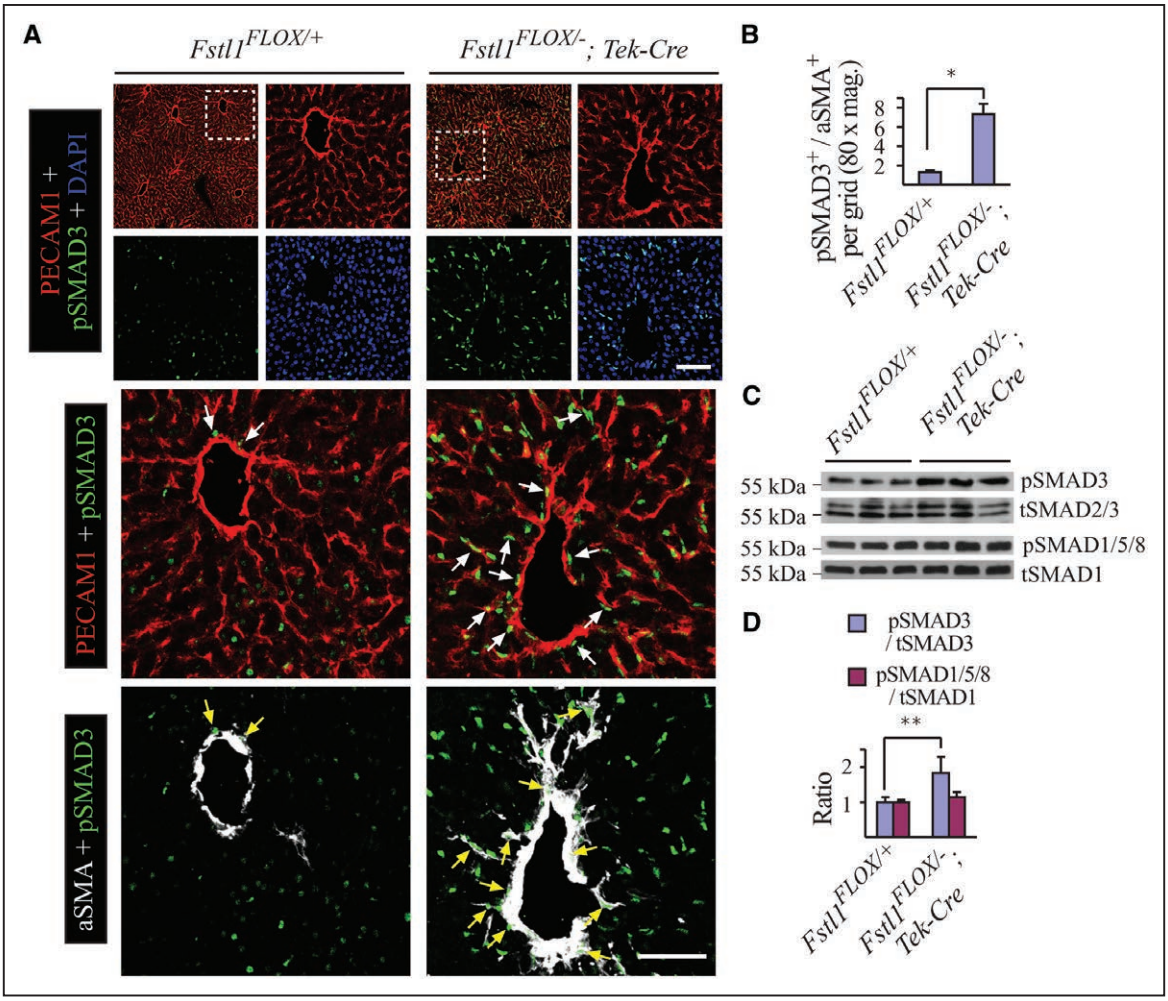

Figure 6. SMAD3 (mothers against decapentaplegic homolog 3) activation in vascular mural cells of *Fstl1*^{ECKO} mutant mice. **A** and **B**, Analysis of pSMAD3 (phosphorylated SMAD3)-positive cells by immunostaining and the quantification of pSMAD3^{+}/αSMA^{+} doubly positive cells (arrows) surrounding blood vessels in *Fstl1*^{ECKO} mutants compared with the littermate control mice (postnatal day 18). **C** and **D**, Western blot analysis of pSMAD3 and pSMAD1/5/8 in liver tissues (**C**; tSMAD3, total SMAD3; tSMAD1, total SMAD1) and the quantification of the ratio of phosphorylated and total proteins were shown in **D**. Scale bar: 50 μm in **A**. αSMA, α-smooth muscle actin; DAPI, 4′,6-diamidino-2-phenylindole; and PECAM1, platelet endothelial cell adhesion molecule-1.

1.0±0.23, n=6; *Fstl1*^{ECKO}: 1.44±0.26, n=7; *P*=0.0140) as well as the immunostaining to detect the pSMAD3^{+}/αSMA^{+} doubly positive cells associated with blood vessels in the lung of the *Fstl1*^{ECKO} mice (Figure VIIIA in the Data Supplement). However, there was no obvious difference detected with the pSMAD2 level between the *Fstl1*^{ECKO} and littermate control mice (Figure VIIIB in the Data Supplement). Consistent with the above findings in the liver, there was no significant difference observed with pSMAD1/5/8: tSMAD1 in the lung (*Fstl1*$^{Flox/+}$: 1.0±0.31, n=6; *Fstl1*^{ECKO}: 1.08±0.40, n=6; *P*=0.5338).

Amelioration of the Cardiovascular-Associated Fibrosis of *Fstl1*^{ECKO} Mice by the Suppression of TGFβ Pathway

To further verify the involvement of TGFβ pathway in the vascular abnormality after the EC-specific deletion of *Fstl1*, the *Fstl1*^{ECKO} mice were treated with an inhibitor for TGFβ type I receptor kinase (SB431542). As the majority of *Fstl1*^{ECKO} mice will die before 3-week-old, all the treated and control mice were sacrificed at P16 for analysis. As shown in Figure 7, the treatment led to a suppression of SMAD3 activation in the liver of *Fstl1* mutants as shown by the Western blot analysis and also immunostaining (Figure 7A through 7C; pSMAD3 / tSMAD3: WT control with solvent, 1.0±0.12, n=11; *Fstl1*^{ECKO} with solvent, 1.84±0.48, n=10; *Fstl1*^{ECKO} with SB431542, 1.19±0.23, n=10; WT control solvent *versus* *Fstl1*^{ECKO} solvent: *P*<0.0001; *Fstl1*^{ECKO} solvent versus *Fstl1*^{ECKO} SB431542: *P*=0.0478; WT control solvent versus *Fstl1*^{ECKO} SB431542: *P*=0.2424; Dunn multiple comparisons test). The partial inhibition of TGFβ signaling resulted in a significant decrease of blood vessel-associated αSMA (Figure 7D and 7E; αSMA/β-actin: WT control with solvent, 1.0±0.3, n=11; *Fstl1*^{ECKO} with

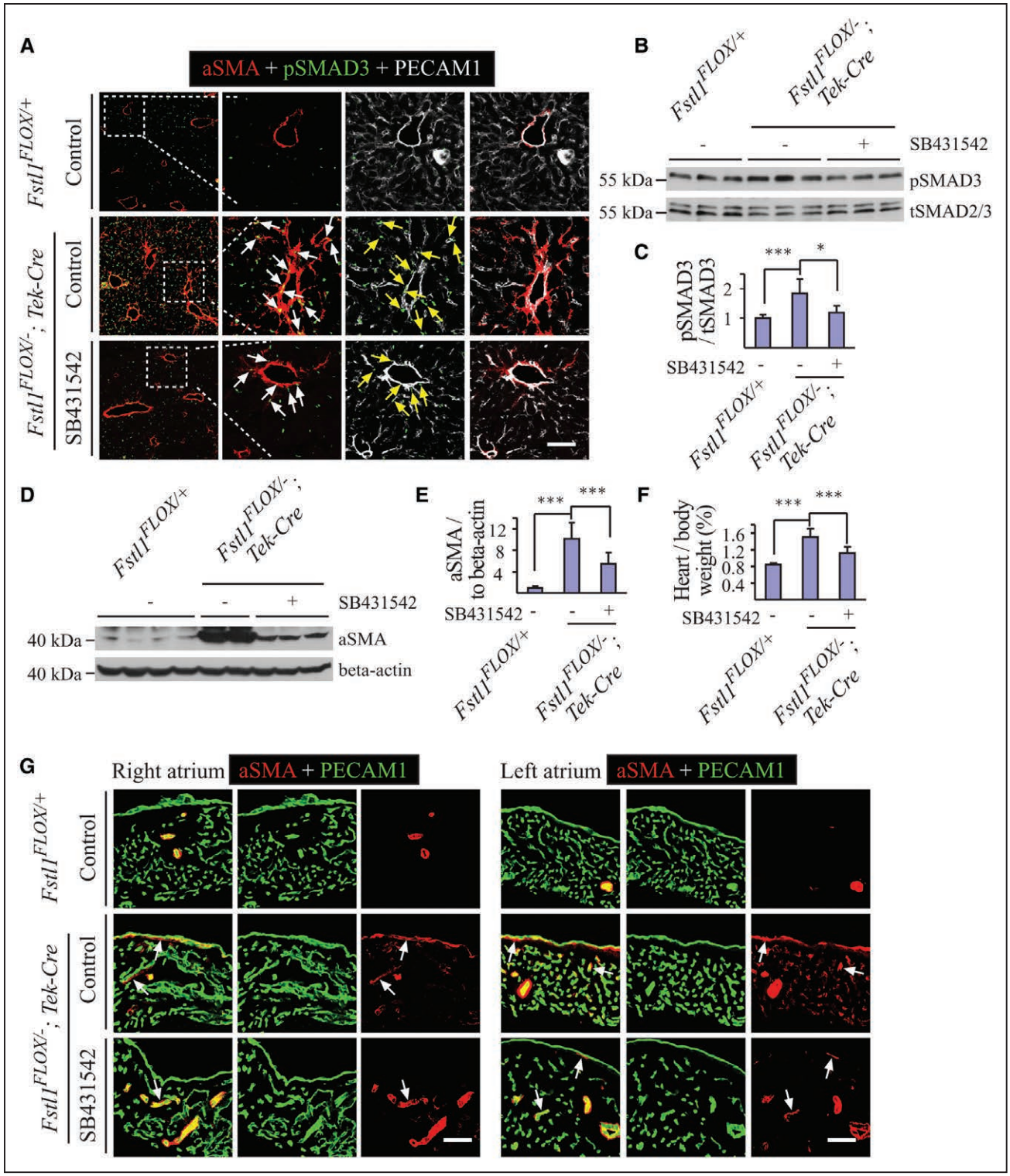

Figure 7. Suppression of TGFβ (transforming growth factor β) signaling ameliorated the cardiovascular-associated fibrosis of *Fstl1*^{ECKO} mutant mice.

A, Immunohistochemical analysis of pSMAD3^{+} (phosphorylated SMAD3)/αSMA^{+} doubly positive cells (white arrows) surrounding blood vessels in the *Fstl1*^{ECKO} mutants treated with the TGFβ pathway inhibitor (SB431542), and the *Fstl1*^{ECKO}, as well as wild-type mice receiving the solvent, were used as controls (P16). Yellow arrows point to the pSMAD3^{+} cells surrounding the PECAM1 (platelet endothelial cell adhesion molecule-1)$^{+}$ blood vessels. **B**–**E**, Western blot analysis of pSMAD3 (**B**) and αSMA (**D**) in liver tissues of the *Fstl1*^{ECKO} mice after the treatment with the TGFβ pathway inhibitor (tSMAD3, total SMAD3; **C**). The quantification of pSMAD3 / tSMAD3 and αSMA / β-actin ratios was shown in **C** and **E,** respectively. **F** and **G**, Immunostaining analysis of blood vessels for PECAM1 (green) and αSMA (red) with right and left atria of the *Fstl1*^{ECKO} mice after the partial suppression of TGFβ signaling. Quantification of the heart to body weight was shown in **F**. Scale bar: 50 μm in **A** and **G**. αSMA indicates α-smooth muscle actin.

solvent, 10.16±2.94, n=9; *Fstl1*^{ECKO} with SB431542, 5.46±2.16, n=9; WT control solvent versus *Fstl1*^{ECKO} solvent: $P<0.0001$; *Fstl1*^{ECKO} solvent versus *Fstl1*^{ECKO} SB431542: $P=0.0001$; WT control solvent versus *Fstl1*^{ECKO} SB431542: $P=0.0001$; Tukey multiple comparisons test). Consistently, there was a significant decrease of the heart to body weight ratio in the treatment group compared with the untreated *Fstl1*^{ECKO} mutants (Figure 7F; WT control with solvent, 0.84±0.04%, n=10; *Fstl1*^{ECKO} with solvent, 1.51±0.20%, n=9; *Fstl1*^{ECKO} with SB431542, 1.12±0.14%, n=10; WT control solvent versus *Fstl1*^{ECKO} solvent: $P<0.0001$; WT control solvent versus *Fstl1*^{ECKO} SB431542: $P=0.0003$; *Fstl1*^{ECKO} solvent versus *Fstl1*^{ECKO} SB431542: $P<0.0001$; Tukey multiple comparisons test). The abnormal association αSMA with the endocardia was almost undetectable in both right and left atria of the treated *Fstl1*^{ECKO} mice compared with the controls (Figure 7G).

DISCUSSION

We have shown in this study that the EC-derived FSTL1 is required for the homeostasis of cardiovascular system. Lack of endothelial FSTL1 led to a dramatic increase of αSMA association with veins and microvessels, in addition to the abnormal remodeling with atrial endocardia as well as heart valves. The excessive αSMA would promote the cardiac rigidity and decrease the vascular elasticity. This may directly account for the alteration of vascular resistance, as reflected by the occurrence of tricuspid regurgitation and the heart failure of the EC-specific *Fstl1* mutant mice. Mechanistically, enhanced activation of SMAD3 signaling was detected in vascular mural cells in the absence of endothelial FSTL1, whereas the SMAD1/5/8 pathway was not obviously affected. Consistently, treatment with a TGFβ pathway inhibitor ameliorated the cardiovascular fibrosis of *Fstl1*^{ECKO} mice, suggesting a negative role of FSTL1 in the regulation of TGFβ-mediated signaling.

It was previously reported that deletion of FSTL1 led to the abnormal development of mitral valves.[30] It is worth noting that the Tek-Cre line (also known as TIE2-Cre) used in our study was shown to have recombinase activity in ECs and also hematopoietic cells.[33,34] With the different Tie2-Cre transgenic mice used by Prakash et al,[30] the Cre recombinase–mediated gene recombination occurred not only in ECs but also in mesenchymal cells of atrioventricular canal and the proximal cardiac outflow tract.[42] It is likely that the defects with mitral valves observed by Prakash et al[30] were at least partly due to the loss of FSTL1 in mesenchymal cells.[30] In this study, we found that the tricuspid valves displayed a more severe abnormality with the regurgitation detected earlier than that of mitral valves. We speculate that the lethality of *Fstl1*^{ECKO} mice in our study may result from the abnormal remodeling of cardiovascular system on a systemic level. First, the excessive αSMA^{+} cell investment with vessel walls detected in several organs would increase the peripheral vascular resistance. Second, the increased association of αSMA with atrial endocardia and heart valves would increase the cardiac rigidity. Both factors would ultimately contribute to the hypertension and heart failure of *Fstl1*^{ECKO} mutant mice.

Pathogenesis of pulmonary hypertension often involves the abnormal vascular muscularization affecting mainly arterioles, such as the increased proliferation of vascular SMCs.[43,44] It has been shown that TGFβ mediated signaling is implicated in the development of pulmonary hypertension, with genetic mutations identified in several genes of this pathway, including ALK1, BMPR2, endoglin, BMP9, and the downstream mediators.[45–47] BMPR2 haploinsufficiency was shown to cause pulmonary arterial hypertension,[48] whereas overexpression of BMPR2 (bone morphogenetic protein receptor type II) in ECs ameliorated pulmonary arterial hypertension via the suppression of Smad2/3 signaling.[49] Furthermore, targeted disruption of SMAD3 signaling suppressed the pathological processes of vascular or interstitial fibrosis in several other organs examined.[50–53] FSTL1 is a TGFβ inducible factor.[16] We found in this study that the endothelial FSTL1 deficiency led to a significant increase of SMAD3 activation but only a mild change with SMAD1/5/8 phosphorylation, suggesting a negative effect of FSTL1 on TGFβ pathway. Consistently, we observed that there was an upregulation of αSMA expression in the cardiovascular system, which may account for the occurrence of hypertension in *Fstl1*^{ECKO} mutants. The alteration of vascular resistance in *Fstl1*^{ECKO} mice was also reflected by the decrease of luminally expressed endomucin in venous and capillary endothelia, as fluid shear stress was shown to downregulate its surface localization.[41] Surprisingly, we found in this study that the increase of αSMA mainly occurred with atria and vein-associated vessels, which was accompanied by the increased collagen deposition as demonstrated in the liver and other tissues, a typical feature of tissue fibrosis. It is possible that EC-derived FSTL1 may maintain the quiescence of peri-endothelium/peri-endocardium mural cells or mesenchymal cells by antagonizing TGFβ signaling. It remains to be investigated about the mechanism underlying the discrepancy among tissues, including veins versus arteries, in response to the loss of endothelial FSTL1. Furthermore, it is unclear why the abnormal vascular remodeling occurred postnatally with *Fstl1*^{ECKO} mice but without any obvious abnormalities observed during embryogenesis, even in *Fstl1* conventional knockout mice (our unpublished observation).

In addition, FSTL1 is expressed also by vascular mural cells, and the muscle-derived FSTL1 was shown to have beneficial effects on cardiovascular functions or tissue

repair in pathological conditions such as pressure overload or injury.[18,19] However, we found that deletion of FSTL1 in SMCs did not affect blood vascular formation and remodeling at 3-week-old when most of the *Fstl1*^{ECKO} mice showed lethality in this study. This is consistent with the recent finding that FSTL1 from different cell-types (eg, myocardial versus epicardial cells) exerts distinct functions in heart, which may be due to the differential protein glycosylation.[21] Further studies are required for providing mechanistic insights into this.

To summarize, the requirement of EC-derived FSTL1 for vascular homeostasis adds a new factor to the regulatory network for vascular health. It is still to be investigated about the differential effects of EC- versus SMC-derived FSTL1 on vascular maintenance and the distinct requirement of endothelial FSTL1 in different organs. Furthermore, this study also introduced a genetically modified disease model for the investigation of mechanisms underlying pathological heart remodeling related to pulmonary or systemic hypertension.

ARTICLE INFORMATION

Received May 21, 2019; accepted February 2, 2020.

Affiliations

From the Cyrus Tang Hematology Center, Collaborative Innovation Center of Hematology, National Clinical Research Center for Hematologic Diseases, State Key Laboratory of Radiation Medicine and Protection, Cam-Su Genomic Resources Center, Soochow University, Suzhou, China (H.J., L.Z., X. Liu, C.C., X. Li, T.L., Z.S., Y.H.); MOE Key Laboratory for Model Animal and Disease Study, Model Animal Research Institute, Nanjing University, China (L.Z., W.S., W.H., F.Z., Q.X., Z.Y., X.G.); Department of Cardiology, The First Affiliated Hospital of Nanjing Medical University, China (W.S.); Max-Planck-Institute for Molecular Biomedicine, Department of Tissue Morphogenesis, and University of Münster, Faculty of Medicine, Germany (K.K., R.H.A.); Department of Cardiology, Nagoya University Hospital, Japan (K.K.); Interdisciplinary Research Center on Biology and Chemistry, Shanghai Institute of Organic Chemistry, Chinese Academy of Sciences, China (J.H.); The First Affiliated Hospital of Zhengzhou University, Academy of Medical Sciences, Zhengzhou University, China (Z.Q.).

Current address for C. Chen: Graduate Program in Genetics, Department of Physiology and Biophysics, Stony Brook University, NY.

Acknowledgments

We thank Drs Rodrigo Dieguez-Hurtado, Cong Xu, and Qi Chen of Max-Planck-Institute for Molecular Biomedicine for helpful discussion about the project and staff in the Animal facility of Soochow University and Model Animal Research Institute of Nanjing University for technical assistance.

Sources of Funding

This work was supported by grants from the National Natural Science Foundation of China (31970768, 81770489, 91739304), the Key Program of Natural Science Foundation of Jiangsu Higher Education Institutions (18KJA180012), the Ministry of Science and Technology of China (YFA0801100), and the Priority Academic Program Development of Jiangsu Higher Education Institutions.

Disclosures

Y. He, H. Jiang, and L. Zhang have a patent application on FSTL1 (follistatin-like protein 1) submitted to the National Intellectual Property Administration, People's Republic of China (application number: 2016100818758). The other authors report no conflicts.

REFERENCES

1. Rafii S, Butler JM, Ding BS. Angiocrine functions of organ-specific endothelial cells. *Nature*. 2016;529:316–325. doi: 10.1038/nature17040
2. Levéen P, Pekny M, Gebre-Medhin S, Swolin B, Larsson E, Betsholtz C. Mice deficient for PDGF B show renal, cardiovascular, and hematological abnormalities. *Genes Dev*. 1994;8:1875–1887. doi: 10.1101/gad.8.16.1875
3. Soriano P. Abnormal kidney development and hematological disorders in PDGF beta-receptor mutant mice. *Genes Dev*. 1994;8:1888–1896. doi: 10.1101/gad.8.16.1888
4. Armulik A, Genové G, Betsholtz C. Pericytes: developmental, physiological, and pathological perspectives, problems, and promises. *Dev Cell*. 2011;21:193–215. doi: 10.1016/j.devcel.2011.07.001
5. Gaengel K, Genové G, Armulik A, Betsholtz C. Endothelial-mural cell signaling in vascular development and angiogenesis. *Arterioscler Thromb Vasc Biol*. 2009;29:630–638. doi: 10.1161/ATVBAHA.107.161521
6. Carvalho RL, Itoh F, Goumans MJ, Lebrin F, Kato M, Takahashi S, Ema M, Itoh S, van Rooijen M, Bertolino P, et al. Compensatory signalling induced in the yolk sac vasculature by deletion of TGFbeta receptors in mice. *J Cell Sci*. 2007;120(pt 24):4269–4277. doi: 10.1242/jcs.013169
7. Larrivée B, Prahst C, Gordon E, del Toro R, Mathivet T, Duarte A, Simons M, Eichmann A. ALK1 signaling inhibits angiogenesis by cooperating with the Notch pathway. *Dev Cell*. 2012;22:489–500. doi: 10.1016/j.devcel.2012.02.005
8. Oh SP, Seki T, Goss KA, Imamura T, Yi Y, Donahoe PK, Li L, Miyazono K, ten Dijke P, Kim S, et al. Activin receptor-like kinase 1 modulates transforming growth factor-beta 1 signaling in the regulation of angiogenesis. *Proc Natl Acad Sci U S A*. 2000;97:2626–2631. doi: 10.1073/pnas.97.6.2626
9. Li DY, Sorensen LK, Brooke BS, Urness LD, Davis EC, Taylor DG, Boak BB, Wendel DP. Defective angiogenesis in mice lacking endoglin. *Science*. 1999;284:1534–1537. doi: 10.1126/science.284.5419.1534
10. Yang X, Castilla LH, Xu X, Li C, Gotay J, Weinstein M, Liu PP, Deng CX. Angiogenesis defects and mesenchymal apoptosis in mice lacking SMAD5. *Development*. 1999;126:1571–1580.
11. Li F, Lan Y, Wang Y, Wang J, Yang G, Meng F, Han H, Meng A, Wang Y, Yang X. Endothelial Smad4 maintains cerebrovascular integrity by activating N-cadherin through cooperation with Notch. *Dev Cell*. 2011;20:291–302. doi: 10.1016/j.devcel.2011.01.011
12. Samarakoon R, Overstreet JM, Higgins PJ. TGF-β signaling in tissue fibrosis: redox controls, target genes and therapeutic opportunities. *Cell Signal*. 2013;25:264–268. doi: 10.1016/j.cellsig.2012.10.003
13. Wynn TA, Ramalingam TR. Mechanisms of fibrosis: therapeutic translation for fibrotic disease. *Nat Med*. 2012;18:1028–1040. doi: 10.1038/nm.2807
14. Harvey A, Montezano AC, Lopes RA, Rios F, Touyz RM. Vascular fibrosis in aging and hypertension: molecular mechanisms and clinical implications. *Can J Cardiol*. 2016;32:659–668. doi: 10.1016/j.cjca.2016.02.070
15. Schafer S, Viswanathan S, Widjaja AA, Lim WW, Moreno-Moral A, DeLaughter DM, Ng B, Patone G, Chow K, Khin E, et al. IL-11 is a crucial determinant of cardiovascular fibrosis. *Nature*. 2017;552:110–115. doi: 10.1038/nature24676
16. Shibanuma M, Mashimo J, Mita A, Kuroki T, Nose K. Cloning from a mouse osteoblastic cell line of a set of transforming-growth-factor-beta 1-regulated genes, one of which seems to encode a follistatin-related polypeptide. *Eur J Biochem*. 1993;217:13–19. doi: 10.1111/j.1432-1033.1993.tb18212.x
17. Adams D, Larman B, Oxburgh L. Developmental expression of mouse Follistatin-like 1 (Fstl1): dynamic regulation during organogenesis of the kidney and lung. *Gene Expr Patterns*. 2007;7:491–500. doi: 10.1016/j.modgep.2006.10.009
18. Miyabe M, Ohashi K, Shibata R, Uemura Y, Ogura Y, Yuasa D, Kambara T, Kataoka Y, Yamamoto T, Matsuo K, et al. Muscle-derived follistatin-like 1 functions to reduce neointimal formation after vascular injury. *Cardiovasc Res*. 2014;103:111–120. doi: 10.1093/cvr/cvu105
19. Shimano M, Ouchi N, Nakamura K, van Wijk B, Ohashi K, Asaumi Y, Higuchi A, Pimentel DR, Sam F, Murohara T, et al. Cardiac myocyte follistatin-like 1 functions to attenuate hypertrophy following pressure overload. *Proc Natl Acad Sci U S A*. 2011;108:E899–E906. doi: 10.1073/pnas.1108559108
20. Sylva M, Moorman AF, van den Hoff MJ. Follistatin-like 1 in vertebrate development. *Birth Defects Res C Embryo Today*. 2013;99:61–69. doi: 10.1002/bdrc.21030
21. Wei K, Serpooshan V, Hurtado C, Diez-Cuñado M, Zhao M, Maruyama S, Zhu W, Fajardo G, Noseda M, Nakamura K, et al. Epicardial FSTL1 reconstitution regenerates the adult mammalian heart. *Nature*. 2015;525:479–485. doi: 10.1038/nature15372
22. Oshima Y, Ouchi N, Sato K, Izumiya Y, Pimentel DR, Walsh K. Follistatin-like 1 is an Akt-regulated cardioprotective factor that is secreted by the heart. *Circulation*. 2008;117:3099–3108. doi: 10.1161/CIRCULATIONAHA.108.767673
23. Lara-Pezzi E, Felkin LE, Birks EJ, Sarathchandra P, Panse KD, George R, Hall JL, Yacoub MH, Rosenthal N, Barton PJ. Expression of follistatin-related genes is altered in heart failure. *Endocrinology*. 2008;149:5822–5827. doi: 10.1210/en.2008-0151

24. Ouchi N, Oshima Y, Ohashi K, Higuchi A, Ikegami C, Izumiya Y, Walsh K. Follistatin-like 1, a secreted muscle protein, promotes endothelial cell function and revascularization in ischemic tissue through a nitric-oxide synthase-dependent mechanism. *J Biol Chem*. 2008;283:32802–32811. doi: 10.1074/jbc.M803440200
25. Liu S, Shen H, Xu M, Liu O, Zhao L, Liu S, Guo Z, Du J. FRP inhibits ox-LDL-induced endothelial cell apoptosis through an Akt-NF-{kappa}B-Bcl-2 pathway and inhibits endothelial cell apoptosis in an apoE-knockout mouse model. *Am J Physiol Endocrinol Metab*. 2010;299:E351–E363. doi: 10.1152/ajpendo.00005.2010
26. Xu J, Qi X, Gong J, Yu M, Zhang F, Sha H, Gao X. Fstl1 antagonizes BMP signaling and regulates ureter development. *PLoS One*. 2012;7:e32554. doi: 10.1371/journal.pone.0032554
27. Sylva M, Li VS, Buffing AA, van Es JH, van den Born M, van der Velden S, Gunst Q, Koolstra JH, Moorman AF, Clevers H, et al. The BMP antagonist follistatin-like 1 is required for skeletal and lung organogenesis. *PLoS One*. 2011;6:e22616. doi: 10.1371/journal.pone.0022616
28. Geng Y, Dong Y, Yu M, Zhang L, Yan X, Sun J, Qiao L, Geng H, Nakajima M, Furuichi T, et al. Follistatin-like 1 (Fstl1) is a bone morphogenetic protein (BMP) 4 signaling antagonist in controlling mouse lung development. *Proc Natl Acad Sci U S A*. 2011;108:7058–7063. doi: 10.1073/pnas.1007293108
29. Tanaka M, Murakami K, Ozaki S, Imura Y, Tong XP, Watanabe T, Sawaki T, Kawanami T, Kawabata D, Fujii T, et al. DIP2 disco-interacting protein 2 homolog A (Drosophila) is a candidate receptor for follistatin-related protein/follistatin-like 1–analysis of their binding with TGF-β superfamily proteins. *FEBS J*. 2010;277:4278–4289. doi: 10.1111/j.1742-4658.2010.07816.x
30. Prakash S, Borreguero LJJ, Sylva M, Flores Ruiz L, Rezai F, Gunst QD, de la Pompa JL, Ruijter JM, van den Hoff MJB. Deletion of Fstl1 (Follistatin-Like 1) from the endocardial/endothelial lineage causes mitral valve disease. *Arterioscler Thromb Vasc Biol*. 2017;37:e116–e130. doi: 10.1161/ATVBAHA.117.309089
31. Li KC, Zhang FX, Li CL, Wang F, Yu MY, Zhong YQ, Zhang KH, Lu YJ, Wang Q, Ma XL, et al. Follistatin-like 1 suppresses sensory afferent transmission by activating Na+,K+-ATPase. *Neuron*. 2011;69:974–987. doi: 10.1016/j.neuron.2011.01.022
32. Lakso M, Pichel JG, Gorman JR, Sauer B, Okamoto Y, Lee E, Alt FW, Westphal H. Efficient *in vivo* manipulation of mouse genomic sequences at the zygote stage. *Proc Natl Acad Sci U S A*. 1996;93:5860–5865. doi: 10.1073/pnas.93.12.5860
33. Koni PA, Joshi SK, Temann UA, Olson D, Burkly L, Flavell RA. Conditional vascular cell adhesion molecule 1 deletion in mice: impaired lymphocyte migration to bone marrow. *J Exp Med*. 2001;193:741–754. doi: 10.1084/jem.193.6.741
34. Payne S, De Val S, Neal A. Endothelial-specific cre mouse models. *Arterioscler Thromb Vasc Biol*. 2018;38:2550–2561. doi: 10.1161/ATVBAHA.118.309669
35. Wu Z, Yang L, Cai L, Zhang M, Cheng X, Yang X, Xu J. Detection of epithelial to mesenchymal transition in airways of a bleomycin induced pulmonary fibrosis model derived from an alpha-smooth muscle actin-Cre transgenic mouse. *Respir Res*. 2007;8:1. doi: 10.1186/1465-9921-8-1
36. de Boer J, Williams A, Skavdis G, Harker N, Coles M, Tolaini M, Norton T, Williams K, Roderick K, Potocnik AJ, et al. Transgenic mice with hematopoietic and lymphoid specific expression of Cre. *Eur J Immunol*. 2003;33:314–325. doi: 10.1002/immu.200310005
37. Chakraborty R, Saddouk FZ, Carrao AC, Krause DS, Greif DM, Martin KA. Promoters to Study Vascular Smooth Muscle. *Arterioscler Thromb Vasc Biol*. 2019;39:603–612. doi: 10.1161/ATVBAHA.119.312449
38. Diéguez-Hurtado R, Kato K, Giaimo BD, Nieminen-Kelhä M, Arf H, Ferrante F, Bartkuhn M, Zimmermann T, Bixel MG, Eilken HM, et al. Loss of the transcription factor RBPJ induces disease-promoting properties in brain pericytes. *Nat Commun*. 2019;10:2817. doi: 10.1038/s41467-019-10643-w
39. Tania NP, Maarsingh H, T Bos IS, Mattiotti A, Prakash S, Timens W, Gunst QD, Jimenez-Borreguero LJ, Schmidt M, van den Hoff MJB, et al. Endothelial follistatin-like-1 regulates the postnatal development of the pulmonary vasculature by modulating BMP/Smad signaling. *Pulm Circ*. 2017;7:219–231. doi: 10.1177/2045893217702340
40. Shah M, Phillips MR, Quintana M, Stupp G, McLean SE. Echocardiography allows for analysis of pulmonary arterial flow in mice with congenital diaphragmatic hernia. *J Surg Res*. 2018;221:35–42. doi: 10.1016/j.jss.2017.06.080
41. Zahr A, Alcaide P, Yang J, Jones A, Gregory M, dela Paz NG, Patel-Hett S, Nevers T, Koirala A, Luscinskas FW, et al. Endomucin prevents leukocyte-endothelial cell adhesion and has a critical role under resting and inflammatory conditions. *Nat Commun*. 2016;7:10363. doi: 10.1038/ncomms10363
42. Kisanuki YY, Hammer RE, Miyazaki J, Williams SC, Richardson JA, Yanagisawa M. Tie2-Cre transgenic mice: a new model for endothelial cell-lineage analysis in vivo. *Dev Biol*. 2001;230:230–242. doi: 10.1006/dbio.2000.0106
43. Tuder RM, Archer SL, Dorfmüller P, Erzurum SC, Guignabert C, Michelakis E, Rabinovitch M, Schermuly R, Stenmark KR, Morrell NW. Relevant issues in the pathology and pathobiology of pulmonary hypertension. *J Am Coll Cardiol*. 2013;62(25 Suppl):D4–12. doi: 10.1016/j.jacc.2013.10.025
44. Voelkel NF, Natarajan R, Drake JI, Bogaard HJ. Right ventricle in pulmonary hypertension. *Compr Physiol*. 2011;1:525–540. doi: 10.1002/cphy.c090008
45. Wang G, Fan R, Ji R, Zou W, Penny DJ, Varghese NP, Fan Y. Novel homozygous BMP9 nonsense mutation causes pulmonary arterial hypertension: a case report. *BMC Pulm Med*. 2016;16:17. doi: 10.1186/s12890-016-0183-7
46. Machado RD, Southgate L, Eichstaedt CA, Aldred MA, Austin ED, Best DH, Chung WK, Benjamin N, Elliott CG, Eyries M, et al. Pulmonary arterial hypertension: a current perspective on established and emerging molecular genetic defects. *Hum Mutat*. 2015;36:1113–1127. doi: 10.1002/humu.22904
47. Goumans MJ, Liu Z, ten Dijke P. TGF-beta signaling in vascular biology and dysfunction. *Cell Res*. 2009;19:116–127. doi: 10.1038/cr.2008.326
48. Machado RD, Pauciulo MW, Thomson JR, Lane KB, Morgan NV, Wheeler L, Phillips JA 3rd, Newman J, Williams D, Galiè N, et al. BMPR2 haploinsufficiency as the inherited molecular mechanism for primary pulmonary hypertension. *Am J Hum Genet*. 2001;68:92–102. doi: 10.1086/316947
49. Harper RL, Reynolds AM, Bonder CS, Reynolds PN. BMPR2 gene therapy for PAH acts via Smad and non-Smad signalling. *Respirology*. 2016;21:727–733. doi: 10.1111/resp.12729
50. Liu R, Das B, Xiao W, Li Z, Li H, Lee K, He JC. A novel inhibitor of homeodomain interacting protein kinase 2 mitigates kidney fibrosis through inhibition of the TGF-beta1/Smad3 pathway. *J Am Soc Nephrol*. 2017;28:2133–2143. doi: 10.1681/ASN.2016080841
51. Sato M, Muragaki Y, Saika S, Roberts AB, Ooshima A. Targeted disruption of TGF-beta1/Smad3 signaling protects against renal tubulointerstitial fibrosis induced by unilateral ureteral obstruction. *J Clin Invest*. 2003;112:1486–1494. doi: 10.1172/JCI19270
52. Wang W, Huang XR, Canlas E, Oka K, Truong LD, Deng C, Bhowmick NA, Ju W, Bottinger EP, Lan HY. Essential role of Smad3 in angiotensin II-induced vascular fibrosis. *Circ Res*. 2006;98:1032–1039. doi: 10.1161/01.RES.0000218782.52610.dc
53. Lee JI, Wright JH, Johnson MM, Bauer RL, Sorg K, Yuen S, Hayes BJ, Nguyen L, Riehle KJ, Campbell JS. Role of Smad3 in platelet-derived growth factor-C-induced liver fibrosis. *Am J Physiol Cell Physiol*. 2016;310:C436–C445. doi: 10.1152/ajpcell.00423.2014Author Queries